Carbon Matrix with Atomic Dispersion of Binary Cobalt/Iron-N Sites as Efficient Peroxymonosulfate Activator for Organic Pollutant Oxidation.

ZHANG, Bofan, LI, Xianquan, BINGHAM, Paul <http://orcid.org/0000-0001-6017-0798>, AKIYAMA, Kazuhiko and KUBUKI, Shiro

Carbon Matrix with Atomic Dispersion of Binary Cobalt/Iron-N Sites as Efficient Peroxymonosulfate Activator for Organic Pollutant Oxidation

Bofan Zhang[1, †, *], Xianquan Li[2, †], Paul A. Bingham[3], Kazuhiko Akiyama[1], Shiro Kubuki[1]

[1]Department of Chemistry, Tokyo Metropolitan University, Tokyo 192-0397, Japan

[2]Dalian Institute of Chemical Physics, Chinese Academy of Sciences, Dalian 116023, China

[3]College of Business, Technology and Engineering, Sheffield Hallam University, Howard Street, Sheffield S1 1WB, UK

*Corresponding author: Bofan Zhang

E-mail: 15054218031@163.com (B.F. Zhang)

† These authors contributed equally

Abstract

Monometallic single atom catalysts have exhibited excellent catalytic capacity due to their unique structural features. However, it remains challenging to promote the limited number of active sites and realize high-efficiency and stability during Fenton-like catalysis. Herein, a nitrogenized graphitic carbon matrix containing Fe-Co dual single atoms (FeCoNC) manifested enhanced catalytic capacity in persulfate activation for tetracycline hydrochloride (TC) oxidation. Nonradical singlet oxygen ($^1O_2$) was identified as dominant reactive species in both FeCoNC and CoNC systems, while the formation pathways of $^1O_2$ and TC catalysis processes were distinct different. ^{57}Fe Mössbauer spectroscopy and theoretical calculations revealed that the dynamic electronic structure and covalency of Fe-N/Co-N bond configuration after coordinating with a second neighboring metal atom induced promoted electron transfer and tuned reactive species transformation pathways. Benefiting from the optimized N_3-Fe-Co-N_3 structure and synergistic effect of dual metal sites, the FeCoNC catalyst was endowed with lowered reaction barriers, adaptability and excellent stability, demonstrating promising practical application potential. This work unveiled the intrinsically regulated mechanism of dual single metal sites towards refractory organic oxidation and delivered enhanced understanding of covalency and electronic configuration on PMS-AOPs based catalysis processes.

Keywords: covalency, dual single atoms, metallic interaction, PMS activation, wastewater

Introduction

Efficient activation of persulfate oxidant to produce reactive oxygen species is essential significance in advanced oxidation processes (AOPs). Peroxymonosulfate (PMS)-dominated Fenton-like reaction is attracting extensive research interest for refractory organic pollutants decontamination. Sulfate radicals ($SO_4^{\bullet-}$, E^0=2.5−3.1 V) with a higher redox potential than that of hydroxyl radicals (•OH, E^0=1.8−2.7 V) can be generated via PMS activation and conversion[1, 2]. Besides, nonradical species such as singlet oxygen ($^1O_2$), high-valent iron complexes and electron transfer pathways were also reported in PMS oxidative system, which displayed highly resistance to the background matrix in aqueous solution[3, 4]. To date, heterogenous catalysts including porous carbon materials, transition metals and their corresponding metal oxides, and noble metals were widely employed in Fenton-like process[5-7]. Efficient redox circulation of transition metal sites has demonstrated its superiority in accelerating PMS conversion and emerged as a potential frontier towards organics oxidation.

Among the various transition metal catalysts, composites containing nitrogen-doped carbon and transition metal (M-N-C) are of particular interest due to their unique electronic structure and maximized metal utilization[8-11]. Recently, multiple N-doped carbon-based single atom catalysts with monoatomic dispersion of Fe, Cu and Mo ions were applied into the Fenton-like reaction, where M-N_x moiety was identified as mainly reactive site towards persulfate activation. For instance, Peng et al.[12] reported that Fe-N_4-C structures engaged as dominant active centers play significant role in antibiotic adsorption. Sun et al[13]. demonstrated that the confinement of N atoms on single Co atoms displayed extremely rapid catalytic rates towards PMS conversion and tetracycline decontamination. Despite the encouraging strategies and exploration, some general issues and challenges remain to be overcome, for example, the inefficient active sites, the block of

active sites by intermediates and thus improved energy barrier for O-O bond cleavage and the weakness of stability of isolated single atom.

Modification of coordination configuration through designing two adjacent isolated atoms may enable optimization of the electronic structure and intrinsic coordination environment of M-N-C catalysts, thus optimizing the activation energy and achieving synergistic metrics[14-18]. Benefitting from unique properties and activation performance towards persulfate, cobalt has drawn considerable research interest during Fenton-like processes due to the suitable standard redox potential (1.82 eV)[13]. The partial substitution of Co atoms with a lower electronegativity metal can control the overall electronic structure and coordination behavior. The deliberate integration Fe atoms with relatively low electronegativity and similar atomic radius in Co-N-C matrix can achieve both geometric and electronic architecture manipulation, which may observably reach the optimal binding affinity with N-C layer and promote multistep Fenton-like catalysis process. Recent work reported that double-atom catalysts showed efficient catalytic performance and were conducive to mass transfer in ORR/OER reaction compared with single-atom catalyst[19, 20]. Therefore, it is reasonable to anticipate that incorporation of Co and Fe atoms can facilitate PMS conversion and compounds oxidation. However, the synergistic relationship and genuine catalytic mechanism behind bimetallic atoms during PMS-AOPs processes should be fully elucidated.

In this work, atomically dispersed dual Fe-Co metal atoms coordinated with N-doped carbon matrix were synthesized using facile pyrolysis strategies. ^{57}Fe Mössbauer spectroscopy, X-ray absorption spectroscopy (XAS) and theoretical calculation (DFT) were used to understand the detailed structure and variation of configuration after doping Fe atoms into Co-N-C moieties. Electron Paramagnetic Resonance (EPR) spectroscopic analysis and scavenging experiments

verified the dominant reactive species of nonradical singlet oxygen ($^1O_2$) in both two systems, whereas the generation pathways were noticeably different from each other. In the N_3-coordinated-N_3 adjacent dual-metal model, the introduced Fe not only serves as reactive sites, but it also acts as a "fence", extending the distance between neighboring N atoms in FeCoNC structures, thus improving the covalency of Co-N bonds and preventing metal agglomeration during carbonization. Iron doping altered the activation mode for PMS, resulting in the increased number of electron transmission for improved breakage of O-O bond in PMS. Such a synergistic effect optimized the electronic density and configuration, which significantly suppressed metal ion leaching and accelerated the catalytic process and catalytic stability.

2 Experimental section

2.1 Chemicals

The details of chemical reagents, materials and characterization are listed in the Supporting Information.

2.2 Synthesis of catalysts

Fe/Co-MOFs were synthesized using a facile solvothermal method. Briefly, certain amount of $FeCl_3 \cdot 6H_2O$ and $Co(NO_3)_2 \cdot 6H_2O$, 5 mmol terephthalic acid were added into 10 mL N, N′-dimethylformamide (DMF) solution. After mixing and stirring for 60 min, the mixture was transferred into a Teflon-lined stainless-steel container and heated at 150 ºC for 3h. Afterwards, the suspension was centrifuged and washed with ethanol and deionized water for six times. Finally, the obtained material was dried at 60 ºC for 12h. Samples synthesized with different Fe/Co ratios of 2:1, 1:1, 1:2 and 0:1 were designated as Fe/Co-MOFs-1, Fe/Co-MOFs-2, Fe/Co-MOFs-3 and Co-MOFs, respectively.

For synthesis of FeCoNC materials, the Fe/Co-MOFs precursor was firstly mixed and ground with melamine at a mass ratio of 1:5. After that, the mixture was transferred into a quartz boat and heated in a tube furnace for 3h at 600 ºC under flowing N_2 gas. After cooling to room temperature, the obtained samples were soaked in 1M H_2SO_4 solution at 80 ºC for 6h. The final obtained black powder samples were named FeCoNC-1, FeCoNC-2, FeCoNC-3 and CoNC.

2.3 Catalytic activity evaluation

The catalytic performance of as-synthesized catalysts was evaluated towards PMS activation for refractory organic pollutant oxidation, including tetracycline hydrochloride (TC), bisphenol A (BPA), carbamazepine (CBZ), methylene blue (MB) and 4-hydroxylbenzoic acid (HBA). Specifically, the as-prepared solid catalyst powder (0.3 g L^{-1}) was added into a representative pollutant solution and was shaken for 60 min under dark conditions to achieve an adsorption-desorption equilibrium. Then, 2mM PMS oxidant was introduced to initiate the Fenton-like reaction. During the catalytic process, 1 mL reaction solution was collected at certain time intervals and filtered for further analysis using high liquid performance chromatography (HPLC) and UV-vis measurement.

3. Results and discussion

3.1 Characterization of atomically dispersed metal atoms

As shown in Figure 1a, XRD patterns for as-synthesized catalysts were similar with two characteristic diffraction peaks at around 26.6º 2θ and 44.7º 2θ assigned to graphitic carbon (JCPDS No.26-1080). This result indicated the carbonaceous nature of FeCoNC catalysts, and meanwhile, no additional peaks assigned to Fe and Co crystals were observed in the diffraction patterns for all catalysts, excluding the existence of metallic and oxidative nanoparticles[21]. From SEM and TEM images (Figure 1d), the FeCoNC catalyst possesses a clear graphitic lamellar structure with abundant nanopores, which was consistent with the X-ray diffraction results. HRTEM images (Figure 1d) showed an amorphous carbon structure without detection of any crystalline Fe and Co species. Besides, numerous double atoms were observed in the marked region in the HAADF-STEM image and the signals of Fe and Co atoms exhibited homogeneously arrangements, which confirmed the existence of dual Fe-Co sites (Figure S2a). The corresponding elemental mapping indicated uniform distribution of Fe and Co atoms in nitrogen-doped carbon layers. Raman spectroscopy was also performed to explore the structural characteristics of as-prepared catalysts. As depicted in Figure 1c, Raman spectra for catalysts exhibited two characteristic peaks located at 1330 and 1580 cm^{-1}, which were assigned to D band and G band. The intensity ratio of these two bands (I_D/I_G) can be used to estimate the graphitization and degree of defects[22]. The gradually increasing I_D/I_G value with introduction of iron elements compared with CoNC material indicated improved structural defect density, such as carbon vacancies and edge defects. The N_2 adsorption-desorption isotherms were further carried out to determine the pore structure and corresponding specific surface area (Figure 1b). The Type-IV isotherms with distinct hysteresis loops corroborate the existence of mesoporous structures in all catalysts. The

corresponding BET specific surface area of samples CoNC, FeCoNC-1, FeCoNC-2 and FeCoNC-3 were calculated to be 116.8, 29.45, 15.36 and 43.24 m^2 g^{-1}, respectively. The pore size distribution curves with their pore volume and pore size were also summarized in Figure S1 and Table S1. The existence of mesopores as well as unique lamellar structures is beneficial to mass transfer during PMS-AOPs based heterogenous catalysis[21].

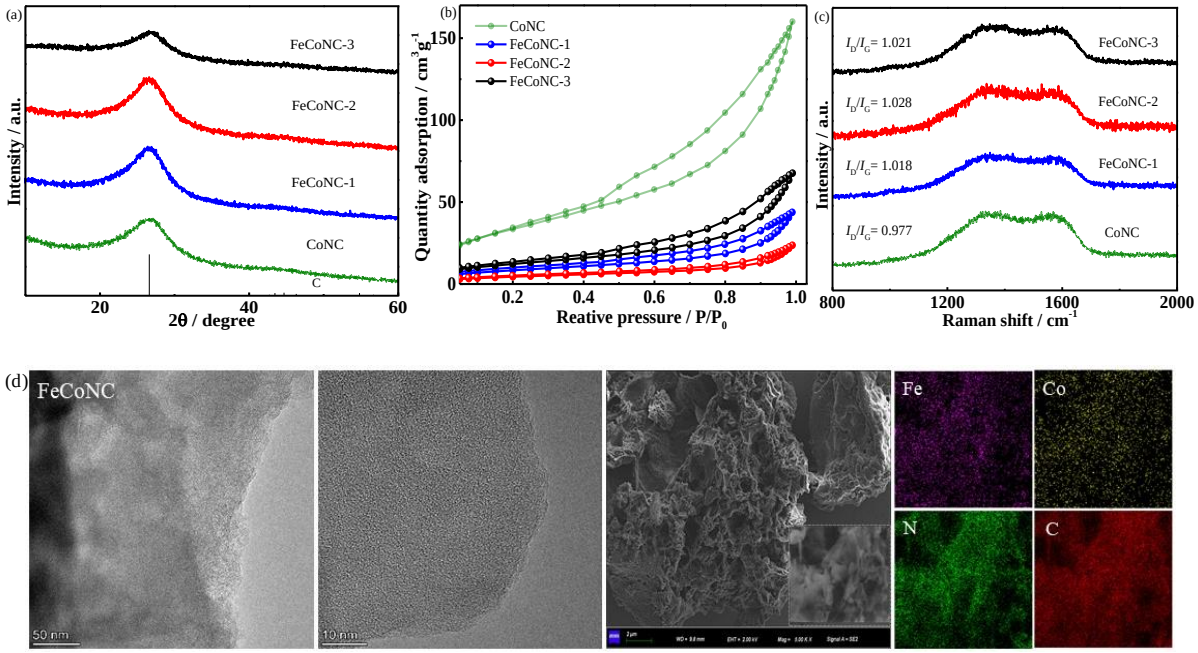

Figure 1. (a) XRD patterns; (b) N_2 adsorption-desorption isotherm; (c) Raman spectra of as-synthesized catalysts; (d) TEM and SEM images of FeCoNC-2 catalyst

The X-ray photoelectron spectroscopy (XPS) spectra revealed the co-existence of Fe, Co, N and C elements (Table S3). The Fe 2p and Co 2p XPS spectra (Figure S2) confirmed the ionic states without observation of metallic sites in all-prepared FeCoNC catalysts. In addition, the higher bonding energy of Co 2p and Fe 2p compared with metallic metal states suggested the presence of ionic Fe^{II}/Fe^{III} and Co^{II}/Co^{III} species, in which the iron and cobalt content were estimated to be 0.45 wt% and 0.36 wt% by ICP-OES measurement. Moreover, the high-resolution N 1s XPS spectra can be divided into four subpeaks at 398.1, 399.2, 400.3 and 403.3 eV (Figure

S3), which were, respectively, assigned to the pyridinic N, pyrrolic N, graphitic N and N-oxide species[23]. Compared with CoNC catalysts, the pyridinic N-peak slightly shifted to lower binding energy and the relative ratio of pyridinic N increased from 48.1% to 55.7% after decoration of Fe atom in FeCoNC catalysts, indicating that pyridinic N was mainly inclined to attach to Fe and Co atoms in the form of coordination bond[24].

The local structural information for iron and cobalt atoms in the FeCoNC catalysts was also investigated via XANES and EXAFS measurements. As depicted in Figure 2c, the normalized Fe K-edge XANES spectrum for sample FeCoNC implied that the absorption edge is located between FeO and Fe_2O_3 references, consistent with a positive valence state of iron species between +2 and +3. Similarly, the Co K-edge XANES spectrum of FeCoNC catalyst situated between CoO and Co_3O_4 references, indicating the positive valence state of Co atom between Co^{2+} and Co^{3+}, which is consistent with the above XPS results. The FT-EXAFS spectrum of sample FeCoNC in Figure 2b-d exhibits prominent peaks at ~1.6 Å and 1.3 Å for Fe and Co K-edges, respectively, which were assigned to Fe-N and Co-N coordination[20]. No available peak corresponding to Co-Co and Fe-Fe bonds can be detected, while a characteristic peak located at 2.3 Å assigned to Fe-Co bond was clearly observed [17], validating the existence of Fe-Co configuration and the atomic dispersion of Fe and Co atoms on the N-doped C support. The slight shift compared to references was attributed to lattice and bond distortion after introduction of hetero-metal sites[20]. The EXAFS fitting parameters for the Fe K–edge spectra give an average Fe coordination number of 3.1 for the first shell (Fe-N) and 1.0 for Fe-Co (Table S4). For the Co atoms, the calculated coordination numbers of Co-Fe (0.9) and Co-N (2.9) suggested a possible structure of N_3-Fe-Co-N_3 moieties in FeCoNC catalysts. The Wavelet transform (WT) plots of data for sample FeCoNC only showed intensity at ~5 $Å^{-1}$, which was ascribed to M-N (M=Fe, Co) configuration[25], further

validating the conclusion that atomically dispersed Fe-Co single atoms were coordinated by N atoms.

^{57}Fe Mössbauer spectroscopy was further conducted to investigate the coordination environment of iron and the variation of metal-ligand bonding induced by the doping iron atoms. Figure 2f-h and Table S5 depicted the ^{57}Fe Mössbauer spectra and the corresponding hyperfine fitting parameters measured at room temperature. Each component was identified by the isomer shift (IS) and quadrupole splitting (QS) that are related to the electron density and the chemical environment near the iron nucleus[26]. It can be observed that all spectra for the FeCoNC catalysts can be only robustly fitted with doublet component. The nonexistence of singlet and sextet could exclude the formation of zero valent iron and/or iron carbide species[27], which is consistent with the XRD and XAS results which indicated that sample FeCoNC consists of atomically dispersed metal atoms. According to the fitting parameters, D1, which possessed relatively high IS and QS values can be assigned to FePc-like $Fe^{II}N$ moieties[27]. By contrast, D2, with an IS value of ~0.4 and a QS value of 0.9-1.0, was originated from $Fe^{III}N$ configurations[28]. It is also noted that the relative ratio of each component was dependent on the doping amount of cobalt atoms, which suggested that the properties are dependent on valence and spin state of the metal sites. It is commonly accepted that the electronic state is sensitive to the Fe-O bond character and Fe-O bond length and covalency can be reasonably estimated by the ^{57}Fe Mössbauer isomer shift (IS) values[29]. In the previously prepared FeNC catalyst, three components with lower IS and QS values than FeCoNC samples manifested the modified electro density and coordination structure[30], especially for the decreased covalency of Fe-N bond and distortion of Fe-N or Co-N bond length with the formation of N_3-Fe-Co-N_3 unit. Specifically, IS as a function of Fe-N bond length at room temperature demonstrated the expanded Fe-N in FeCoNC sample attributed to the

electron charge transfer between Co and Fe atoms. The covalency and its modulation with metal-N bonding in the M-N-C configuration is essential to comprehend the nature of electron-transfer and define electronic structure contributions to the redox ability. Density functional theory (DFT) calculation as a powerful approach can further provide molecular-level perspective of electronic structure and variation. As depicted in Figure 2i and Figure S4, FeCoNC catalyst exhibited a decreased Co-N bond length compared to pristine CoNC sample, which was mainly attributed to the strengthened interaction between Co and N atoms and the enhanced covalent character[31]. Generally, the interatomic space is a typical factor influencing covalency in metallic compounds, whereas Co substitution by transition Fe metal with lower electronegativity may induce a drastic alteration in bond covalency and electronic states. Correspondingly, the electron localization function (ELF), an indicator of the likelihood of detecting electron in the neighborhood electron with same spin located at a certain point[32], also showed the increased covalency of Co-N in FeCoNC sample, highly electron localization and regulated local configuration of metal atoms. Further, in comparison with pristine CoNC catalyst, a higher charge density was observed in sample FeCoNC by charge differential analysis, suggesting that the dual metal sites were more likely to donate electrons to PMS and accelerate the PMS activation process.

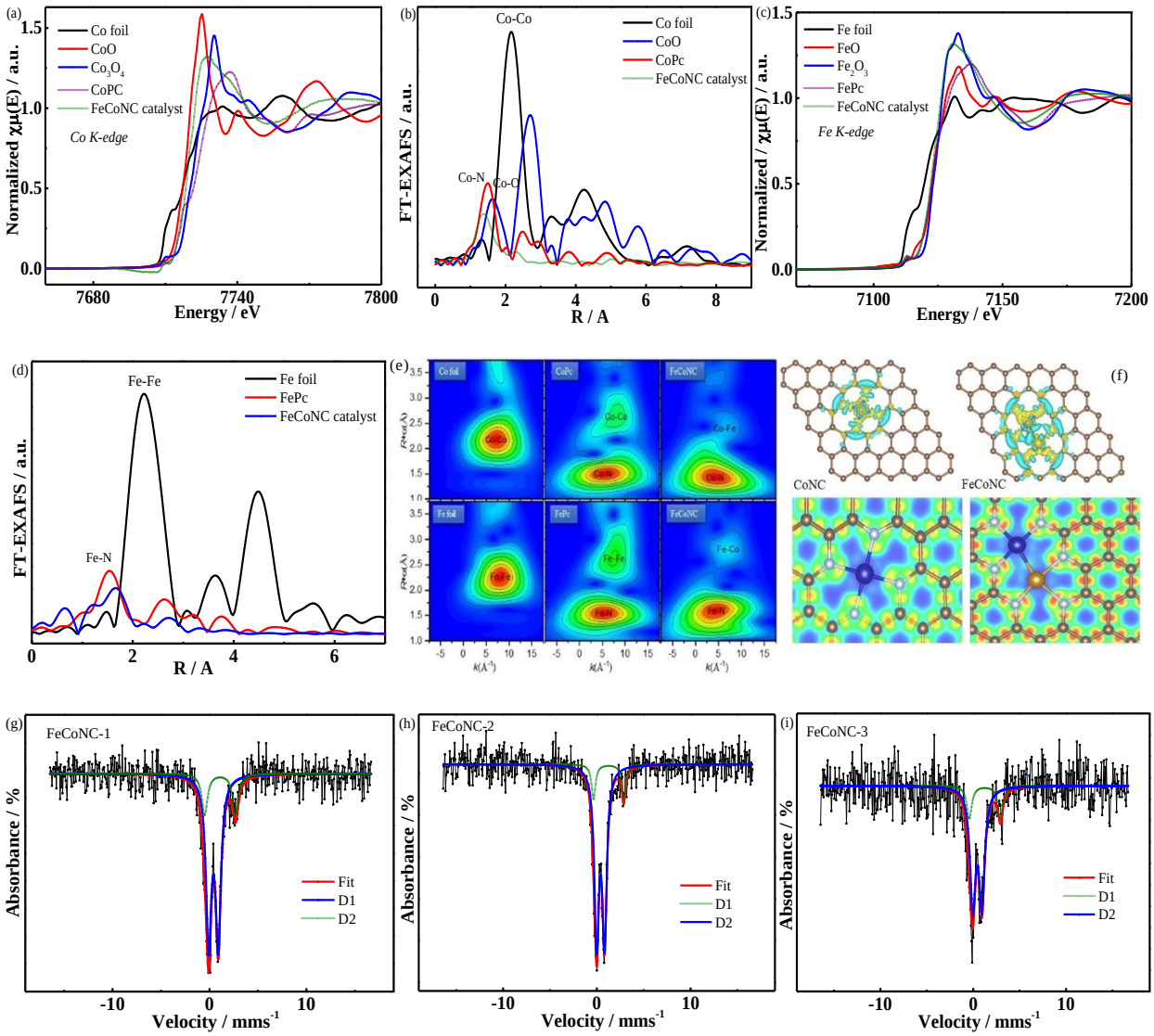

Figure 2. XANES spectra of the (a) Co K-edge XANES, (b) Fourier transform (FT) EXAFS of Co K-edge; (c) Fe K-edge XANES, (d) Fourier transform (FT) EXAFS of Fe K-edge of FeCoNC-2 catalyst; (e) WT-EXAFS of FeCoNC catalysts; (f) The charge-density difference and electron localization functions of CoNC and FeCoNC catalysts; (g-i) ^{57}Fe Mössbauer spectra of FeCoNC catalysts

3.2 FeCoNC catalyst catalyzed PMS activation for removal of organic pollutants

Persulfate activation capacity was investigated using tetracycline hydrochloride (TC, a representative refractory antibiotic pollutant) as a target pollutant. As shown in Figure S5a, the obtained catalysts exhibited negligible TC adsorption capacity in 30 min. Without addition of

single Fe/Co atom catalysts, individual PMS and N-C displayed inappreciable TC degradation efficiency. In contrast, the combination of metal-N-C catalyst and PMS brought about highly TC abatement within 30 mins, indicating excellent PMS activation ability and the prominent role of single metal sites in FeCoNC catalysts. It was noted that the activity of sample FeCoNC-2 towards TC oxidation had been far higher than the other synthesized catalysts in the present work, which was attributed to the significant interrelationship between two isolated metal atoms. Normalizing TC degradation rate constants to catalyst dosages and specific surface areas further identified the optimal specific activity of sample FeCoNC-2 (0.0107 L min^{-1} m^{-2}), followed by sample FeCoNC-3 (0.0029 L min^{-1} m^{-2}), sample FeCoNC-1 (0.0023 L min^{-1} m^{-2}) and sample CoNC (0.0010 L min^{-1} m^{-2}). Further, the FeCoNC-2 sample still exhibited the highest turnover frequency (TOF) value (Table S2), indicating the excellent synergistic effect of suitable Fe/Co ratio and the efficient utilization of metal active sites. In comparison with single isolated site catalyst, the two adjacent metal atoms could modify the electronic structure and provide catalytic synergy by altering activation energy, thus promoting the intrinsic oxidation behavior[33, 34]. These results demonstrated that (i) dual metal sites at atomic precision outperform the mono-metal atom supported catalysts for PMS activation; and (ii) appropriate dual metal site ratios and interactions are at the core of PMS conversion and pollutant oxidation ability. In addition, the influence of various conditional parameters on TC degradation was investigated. As depicted in Figure S5, as the concentration of TC pollutant decreased from 100 mg L^{-1} to 40 mg L^{-1}, the removal efficiency was inclined to be gradually improved. Further, increasing catalyst dosage and PMS concentration also correspondingly promoted the catalysis process. In consideration of economic viability, toxicity and sufficient activity in a representative aquatic environment, the optimal conditions were fixed as follows: 0.3 g L^{-1} catalyst dosage, 2 mM PMS and 80 mg L^{-1} TC pollutant. In these

conditions, the FeCoNC sample can achieve efficient TC oxidation and adaptation over a wide pH range of 4-10. Several common refractory organic pollutants including bisphenol A (BPA) and methylene blue (MB) were completely removed with 30 min and more than 70% of carbamazepine (CBZ) and 4-hydroxybenzoic acid (HBA) can also be degraded, signifying the superior catalytic activity and adaptability of the FeCoNC/PMS system. The excellent mineralization ability was also illustrated by evaluating the total organic carbon (TOC) removal efficiency of these refractory compounds (Figure 3c). The above phenomena collectively indicated the versatile and reliable ability of the FeCoNC-2 catalyst in complex environments and in actual wastewater purification.

Apart from catalytic capacity, long-term stability and reusability of the FeCoNC-2 catalyst were investigated by five cycling experiments. After each cyclic test, the catalyst was filtered to recollect and washed by deionized water and then dried for next usage. As shown in Figure 3d, the catalytic performance of FeCoNC-2 catalyst maintained 92% of its original removal efficiency after consecutive five cycles. The slight attenuation of efficiency in the reusability test may derive from the coverage of partial decomposition intermediates on the catalyst surface and slight loss of Co and Fe ions (the leached total Fe and Co concentrations were determined to be 0.031 and 0.032 mg L^{-1} by ICP-OES measurement). However, the leached Fe and Co ions in the reaction solution were tested to be far below the level needed for heterogenous catalysis, and exhibited an inappreciable contribution to compound oxidation. In addition, the negligible measured variation of crystalline structure of the used FeCoNC-2 sample compared to the pristine sample confirmed there was validated no aggregation of Co and Fe ion species in the N-C matrix, indicating that the FeCoNC catalyst is indeed a promising candidate in the field of environment remediation.

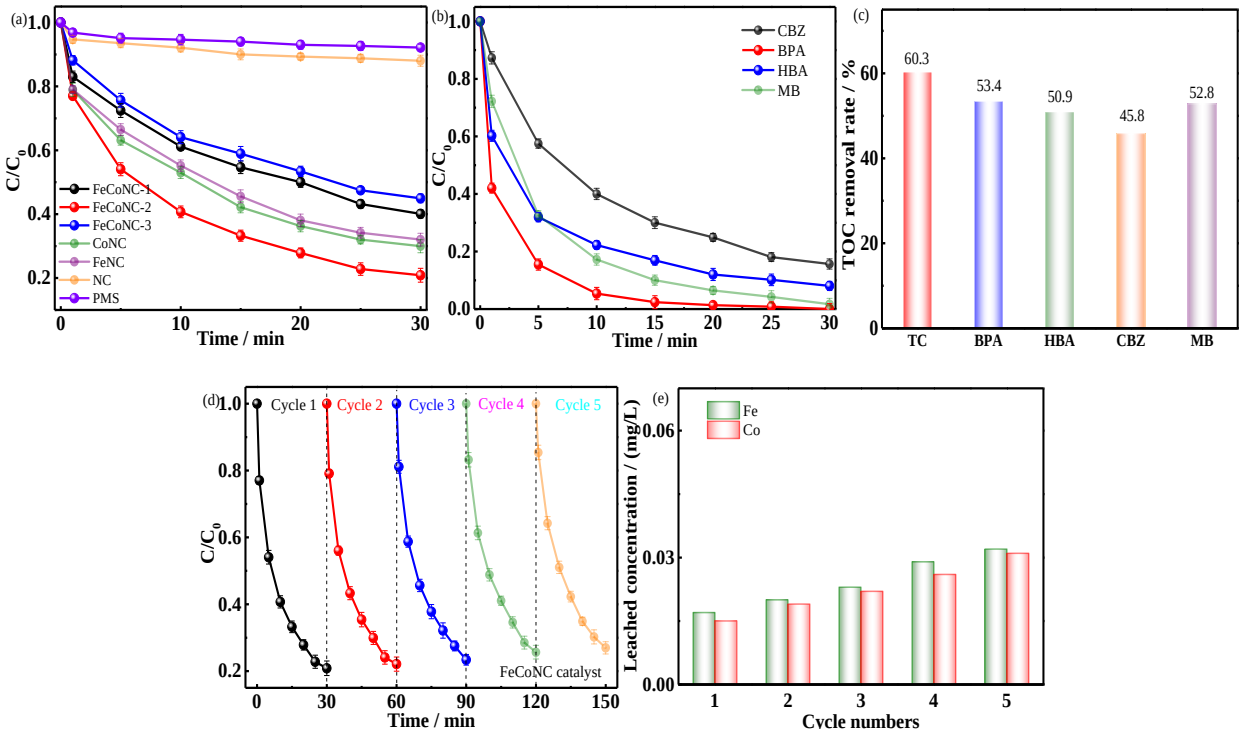

Figure 3. (a) The removal of TC in different reaction systems; (b-c) Catalytic performance towards different organic pollutants in FeCoNC-2/PMS system; (d) The reusability test of FeCoNC-2 for TC degradation; (e) Leached metal concentration after each cyclic experiment; Reaction conditions: catalyst dosage = 0.3 g/L, $[PMS]_0$ = 2.0 mM, $[TC]_0$ = 80 mg/L, $[BPA]_0$ = $[HBA]_0$ = $[CBZ]_0$ = $[MB]_0$ = 20 mg/L;

3.3 Identification of regulated reactive species in FeCoNC and CoNC systems

To elucidate the catalytic mechanism of TC abatement by the FeCoNC/PMS system, the predominant oxidative species contributing to pollutants decomposition were systematically investigated. Methanol and tert-butyl alcohol (TBA) are particular scavengers for $SO_4^{\bullet-}$ (k = 2.5 × 10^7 M^{-1} s^{-1}) and •OH (k = 9.7 × 10^8 M^{-1} s^{-1}), •OH (k = 5.2 × 10^{10} M^{-1} s^{-1}) radicals[35], respectively. As shown in Figure 4a, the addition of TBA did not give rise to significant inhibition and TC can be still completely degraded within 30 min, suggesting the slight contribution of •OH in the FeCoNC/PMS system. In contrast, when MeOH was added into the solution, the removal efficiency was suppressed, which confirmed the important effect of $SO_4^{\bullet-}$ radicals in this case.

Conversely, the unsuppressed TC removal efficiency after introduction of MeOH in the CoNC/PMS system, which behaved differently from the FeCoNC-2 system, indicated differences in reactive species after integration of double metal atoms. Furthermore, EPR spectroscopy was carried out to further identify the radical generation. No signal of $SO_4^{\bullet-}$ and •OH radicals in PMS alone and CoNC/PMS systems was observed, while only relatively weak paramagnetic peaks for DMPO-$SO_4^{\bullet-}$ and DMPO-•OH adducts appeared in the spectrum for FeCoNC-2/PMS after 10 min of reaction. Afterwards, a Furfuryl alcohol (FFA, k = 1.2 × 10^8 M^{-1} s^{-1}) scavenging experiment was performed to ascertain the formation of $^1O_2$ species[12]. As presented in Figure 4a-b, FFA addition derived a significant inhibition of TC removal efficiency in both tested systems and the suppression effect gradually enhanced with increasing FFA additive amount (Figure S6). Meanwhile, the improved EPR triplet peak signal (g=2.0054, α_N=16.9 G) assigned for $^1O_2$[36] was detected in the spectra for FeCoNC and CoNC/PMS systems compared to that of PMS alone, validating the existence of non-radical $^1O_2$ reactive species. Generally, $^1O_2$ can be formed through PMS self-decay (HSO_5^-+SO_5^{2-} → HSO_4^-+SO_4^{2-}+$^1O_2$), PMS activation by ketone functional group in pollutants under alkaline condition and the conversion of $O_2^{\bullet-}$ to $^1O_2$ via proton disproportionation reaction ($O_2^{\bullet-}$+ $HO_2^{\bullet}$ → $^1O_2$+HO_2^-)[37]. A test under N_2 injection was carried out and the result indicated the insignificant influence of N_2 on the TC degradation in FeCoNC and CoNC/PMS systems, ruling out the conversion of $^1O_2$ by dissolved oxygen (Figure S7). Further, the addition of benzoquinone (BQ, k = 2.9 × 10^9 M^{-1} s^{-1}) quencher significantly suppressed the TC degradation efficiency of the CoNC/PMS system. However, it was surprisingly found that when DMPO was employed as an $O_2^{\bullet-}$ radicals trapping agent (Figure S8a), only weakly characteristic DMPO-$O_2^{\bullet-}$ adduct signals (α_N=14.9 G, α_H^{α}=10.38G, α_H^{β}=1.31G) can be detected in CoNC system. Given the relatively low redox potential of $O_2^{\bullet-}$ as -0.33V, it was not easy to

efficiently attack TC by $O_2^{\bullet-}$ radicals in theory, but the addition of BQ indeed suppressed the degradation performance. This phenomenon may originate from the following possible causes: 1) the concentration of superoxide radical is lower than the detection limit; 2) the superoxide radical might be an indispensable intermediate species and has transferred into other species; and / or 3) the superoxide radical has been rapidly consumed by organic compounds. To get a clear and comprehensive cognition of this phenomenon, EPR spectra of TEMP-$^1O_2$ adducts were firstly measured in the existence of BQ quencher. As illustrated in Figure S8, the corresponding $^1O_2$ signal strength decreased after addition of BQ, which was attributed mainly to the suppressed conversion from $O_2^{\bullet-}$ to $^1O_2$. Besides, the twice as strong TEMP-$^1O_2$ signal intensity in the spectrum for CoNC/PMS compared to the spectrum for PMS alone excludes the possibility of PMS self-decay process. Thus, it can be concluded that the generated nonradical $^1O_2$ species played a dominant role in the CoNC/PMS system towards organic pollutant oxidation, whereas $O_2^{\bullet-}$ radicals contributed to the transformation of $^1O_2$. However, in the process of the FeCoNC/PMS reaction, not only can the signal for $O_2^{\bullet-}$ radicals not be detected, but the introduction of BQ did not influence the intensity of the TEMP-$^1O_2$ signal and catalytic efficiency of TC at all, suggesting that $^1O_2$ mainly originated from PMS activation rather than from $O_2^{\bullet-}$ radicals, which was quite distinct from the behavior observed for the CoNC catalyst. Considering the EPR spectra and MeOH scavenger test for the FeCoNC system, it can be concluded that singlet oxygen indeed played an essential role, which was derived from PMS conversion and partial $SO_4^{\bullet-}$ and •OH radicals transformation instead of $O_2^{\bullet-}$. Moreover, $^1O_2$ can live longer in the D_2O system[38] and the catalytic efficiency of TC was promoted compared with the DI water system (Figure S9), further confirming the crucial effect of $^1O_2$ nonradical species.

It was also illustrated that high valent iron species in single iron atom catalysts contributed to the bisphenol A decontamination in our previous work[30], in which the catalyst preparation procedure was similar to this work. Considering the presence of Fe-N or FeCo-N moieties, the formation and catalytic effect of high-valent iron or cobalt complexes should therefore be investigated in this work. As depicted in Figure S10a, the addition of dimethyl sulfoxides (DMSO) terminated the target pollutant TC oxidation. However, through analysis of methyl phenyl sulfoxide (PMSO) consumption and methyl phenyl sulfone ($PMSO_2$) generation by LC-MS measurement, although 30% conversion rate of $PMSO_2$ was achieved by the FeCoNC-2 catalyst (Figure S10b), the PMS system alone still yielded 21% of $PMSO_2$, excluding the contribution of high valent metal-oxo complexes, which was distinctly different from the FeNC/PMS system. To illustrate the inhibited influence of DMSO, the PMS decay tendency was monitored after addition of DMSO. As shown in Figure S10c, the consumption of PMS was significantly promoted in the presence of DMSO compared with the control group, indicating that the inhibited catalytic performance was due to the consumption of PMS by DMSO instead of scavenging effect of high valent metal species. Additionally, electron-transfer pathway was widely reported in the heterogenous PMS-based catalytic process. However, unlike the typical electron transfer illustrated in PMS/SA-FeCN and PDS/biochar systems[37, 39], the chronopotentiometry analysis and PMS decay results (Figure S11) collectively ruled out the existence of electron-transfer routine in FeCoNC-2/PMS system.

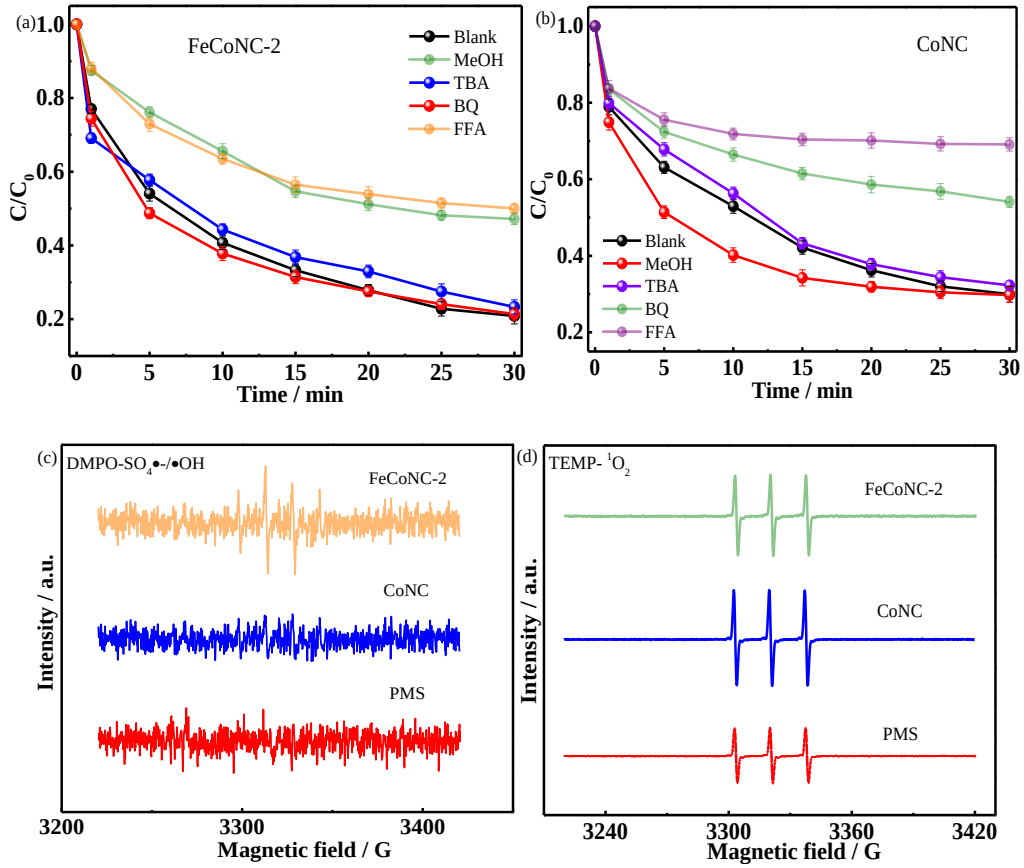

Figure 4. (a-b) Effect of scavengers on TC degradation in FeCoNC-2/PMS and CoNC/PMS systems; (c) EPR spectra of (c) $SO_4^{\bullet-}$ and •OH and (d) $^1O_2$ in various systems; Reaction conditions: catalyst dosage = 0.3 g/L, $[PMS]_0$ = 2.0 mM, $[TC]_0$ = 80 mg/L;

3.4 Exploration of active sites and $FeCoN_6$-mediated catalysis mechanism

Pristine NC material exhibited negligible activity for TC degradation, while strong catalytic performance on PMS and TC by the FeCoNC catalyst was originated from the coordinated cobalt and iron atoms. The presence of oxalate, a quencher of Fe ions[22], suppressed the TC removal efficiency in the FeCoNC/PMS system (Figure S12). Owing to the chelate effect of 1,10-phenanthroline (Phen) towards Fe-N and Co-N moieties instead of carbon-based materials[40], the evidently depressed TC degradation process in the presence of Phen further validated the crucial importance of the Fe/Co-N active centers. To understand the reaction mechanism, the structural and chemical state surveys of FeCoNC catalyst before and after PMS activation were characterized.

As shown in the high-resolution C 1s spectrum of used sample (Figure S3b), no obvious energy shift and the stable ratio of each C species ruled out the contribution of carbon matrixes. By contrast, the pyridinic N content in N 1s high-resolution spectrum decreased from 55.7 to 48.8% after PMS activation, illustrating that the pyridinic N coordinated with metal ions may be the dominant active site. Besides, the amount of graphitic N in used FeCoNC catalyst also decreased from 26.3% to 23.4% due to the fact that graphitic N could delocalize the electron distribution, facilitate the adsorption of oxygen species and then participate into the catalytic reaction[41], which was also reported in previous research. These phenomena suggested that both pyridinic N and graphitic N moieties are likely to be involved in the FeCoNC-catalyzed process. Further, to reveal the specific responsibility of N moiety for PMS accessibility, the correlations between activity and each N species were investigated (Figure S13) and the corresponding results indicated that the catalytic efficiency was found to be mainly positively correlated with pyridinic N species, in accordance with XPS analysis results.

Generally, Fe and Co ions in M-N-C moieties can act as electron donors to cleave peroxide bonds (-O-O-) in PMS. To clearly illustrate bimetallic Fe/Co site catalyzed PMS activation mechanisms, high resolution XPS spectroscopy and ^{57}Fe Mössbauer spectroscopy were employed to clarify the surface chemical environment variation. As shown in Figure S14, the characteristic XPS peaks centered around 710 eV and 724 eV are assigned to Fe $2p_{3/2}$ and Fe $2p_{1/2}$. After reaction, the percentage of Fe^{II} declined from 32.3 to 26.1%, signifying the participation of Fe^{II} sites accompanied by the oxidation into Fe^{III}. In terms of Co 2p spectra, similar tendency of Co valence and proportion was also obtained, confirming the transformation and surface oxidation in Co sites. ^{57}Fe Mössbauer spectroscopy of the used sample showed similar peak profiles to that of fresh one, which can be still fitted with two paramagnetic doublets assignable to the D1 (ferrous Fe^{II}-N) and

D2 (ferric Fe^{III}-N) components (Figure 5a). Further hyperfine parameters reveal that the relative proportion of D1 decreased, accompanied by increased proportion of D2 species after the reaction, indicating the dynamic Fe^{II}/Fe^{III} transformation. Afterwards, *in-situ* Raman spectroscopy was performed to study the catalytic process and surface chemical evolution of Fe/Co-N sites. As depicted in Figure 5b, three characteristic peaks located at 881, 980 and 1060 cm^{-1} were observed in pure PMS solution, which are assigned to the stretching vibration of O-O in HSO_5^- ($[O_3S\text{-}O\text{-}O\text{-}H]^-$), symmetrical SO_4^{2-} stretching vibration and SO_3 vibration in HSO_5^-[42], respectively. The addition of FeCoNC gave rise to an obvious decrease of O-O (HSO_5^-) and SO_3 (HSO_5^-) peak intensity. In the presence of TC pollutant, the distinct vibration peak of O-O (HSO_5^-) almost disappeared and the intensity of PMS significantly declined, suggesting that the contaminant accelerated the PMS activation and conversion by the metal sites in the FeCoNC catalyst through electron transfer to O-O of PMS. Moreover, the dynamic PMS concentration was monitored during the catalytic process and the corresponding attenuation trend of PMS was nearly synchronous with the TC removal tendency, further confirming the efficient PMS conversion process instead of adsorption.

To further shed light on the difference of activation of PMS on the surfaces of monometallic and bimetallic single-atom catalysts, DFT calculation using VASP was conducted and employed to reveal the intrinsic properties of CoNC and FeCoNC catalysts[43]. The total density of sates (DOS) shown in Figure 5 indicated that the electron distribution of sample CoNC was disturbed by the integration of isolated iron atoms, which was conducive to the chemical activity by accelerating electron transfer and modifying the electron distribution. Generally, three types of oxygen atoms, including hydroxy O, peroxy O and terminal O exists in PMS molecule. As reported by Li et.al[32], the predominant absorption configuration was achieved by terminal oxygen atoms

due to the most negative adsorption energy. Herein, the fully relaxed PMS adsorption configurations were also optimized and calculated by bonding metal sites with different charge density. As depicted in Figure 5, the corresponding adsorption energies (E_{ads}) on CoNC and FeCoNC was calculated to be -0.96 and -1.70 eV, indicating the more active adsorption behavior of PMS on bimetallic catalysts. Moreover, the O-O bond length in PMS is around 1.43 Å[38]. When the PMS was adsorbed onto the CoNC and FeCoNC catalysts, the elongation of the O-O bond was calculated to be 1.47Å and 1.56 Å, respectively, further indicating that PMS is prone to interact with FeCoNC moiety due to the enhancing positive charge density of metal sites, which further promote the electron transfer and bond cleavage to generate reactive oxygen species. Considering the improved covalent Co-N bond, the introduction of additional transition metal promoter not only optimized electronic state but also decreased competition between reactants for active sites, making the adsorption of PMS more favorable. It was also demonstrated that the in-plane Fe/Co sites on N_3-Fe-Co-N_3 moieties instead of N_4Fe-CoN_4 can be easily pulled up by reactant adsorption and revert back upon desorption[44], leading to a good reusability. Precisely tuning the level of metal loading is essential to control the binding stability and distance between metal atoms. When the Fe-Co distance is high, the Fe and Co atoms are far apart in an out-of-plane state and the PMS may no longer easily bind to the bridge site, resulting in losing the synergistic effect of dual metal sites and a larger reaction energy barrier to active PMS and pollutant degradation. Herein, the optimal amount of single Fe atom substitution had been employed in the Co-N-C configuration to boost the PMS activation ability. DFT calculation and Mössbauer spectra verified that the lattice distortion is caused by the coexisted Fe and Co which may result in higher Fe-N stretching vibration and increased Co-N covalency, leading a favorable electronic structure of cobalt atoms. The improvement in the overlap between cobalt and nitrogen states lowered the

energy of between Co 3d and N 2p states, enabling tuned reactive species formation pathways and promoted PMS activation ability towards refractory organic pollutants.

Additionally, some electrical properties and charge transfer during the FeCoNC catalyzed PMS/TC process were clarified using electrochemical measurements. In electrochemical impedance spectroscopy (EIS, Figure S15), the smallest semicircle diameter in the Nyquist plot of data for the FeCoNC sample compared with FeNC and CoNC samples indicated the highest conductivity and lowest electron transfer resistance. In the organic decomposition process, TC tend to lose electrons and thereby was oxidized by the reactive metal sites into small intermediates. Therefore, the current and potential of the catalyst would experience certain variations in this oxidation process[45]. As expected, a current response on the FeCoNC wrapped working electrode was detected with the addition of PMS. Further introduction of TC also provoked remarkable enhancement in current density, which was much higher than for the pristine CoNC catalyst. This result further illustrated the modulated electronic configuration and promoted interaction between PMS and metal sites after integration of single Fe atoms on the CoNC catalyst, which exhibited positive reinforcement between these dual metal sites.

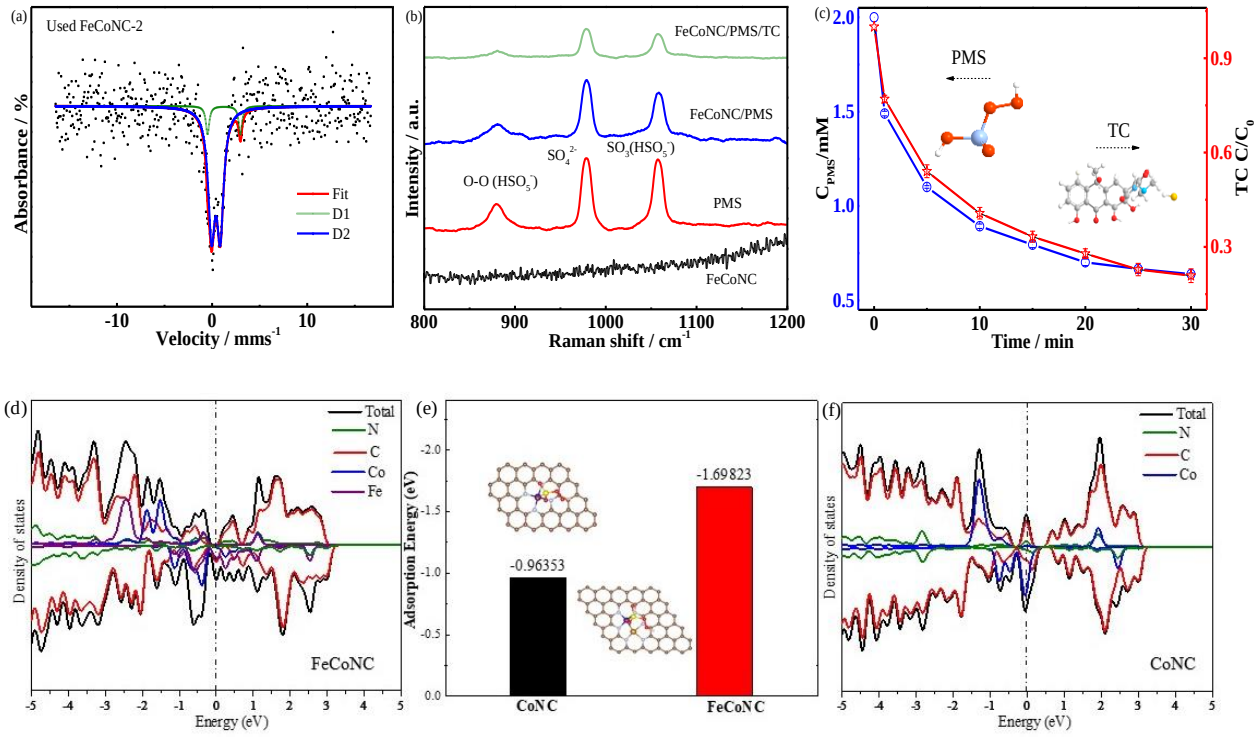

Figure 5. (a) ^{57}Fe Mössbauer spectroscopy of the used FeCoNC sample; (b) *In-situ* Raman spectra of FeCoNC with and without PMS and TC; (c) PMS concentration and TC degradation curve in FeCoNC/PMS system; (d-f) Total density of states (DOS) of each atoms and PMS absorption energy obtained by DFT calculation

3.5 Environmental water application potential

The physicochemical properties of organic compounds can strongly affect their decomposition ability during catalytic processes. Among various descriptors, ionization potential (IP) was reported to closely relate to the redox ability in a specific oxidative system [46]. Herein, the relationship between IP and catalytic rate constant (k) in the FeCoNC/PMS system was plotted in Figure 6a. It was seen that the compounds with IP values higher than the threshold (9.0 eV) cannot be efficiently oxidized, while organics such as BPA, RhB and Phenol with lower IP values were vulnerable to be decomposed with higher catalytic reaction rate. This may be due to electron-donating groups in compounds lowering the IP value, while the electron-withdrawing groups pose

an adverse effect. Recent studies have also demonstrated that the IP value-dependent systems were mainly dominated by nonradical catalyzed pathways rather than free radicals[46, 47], which showed high selectivity towards electron-rich organics. In the present study, this was further corroborated by the existence of singlet oxygen ($^1O_2$), which was identified as a major reactive species towards PMS activation. Considering the regulated reactive species and generation pathway of $^1O_2$ in the CoNC/PMS and FeCoNC/PMS systems, the corresponding organic degradation intermediates may be distinct from each other. Herein, the TC oxidation intermediates catalyzed by these two kinds of catalysts were identified using LC-MS measurement in positive ion mode. As shown in Figures 6b-c and S16, the product with m/z of 445 is assigned to the TC substrate and various degradation intermediates were detected as the reaction time prolonged. The role of $^1O_2$ mediated by CoNC/PMS resulted in larger molecular weight molecules (m/z = 495, 477, 466, 461) by oxygen oxidation due to the conversion of relatively low redox potential of $O_2^{\bullet-}$ into $^1O_2$ [48]. In contrast, the FeCoNC/PMS system mainly undergo dihydroxylation, deamidation and ring-opening reactions[49, 50] to generate numerous small molecules (m/z =387, 311, 212, 211, 190, 175) due to the different transformation derived from $SO_4^{\bullet-}$ and •OH radicals and the auxiliary effect of these radicals (Figure 6g), which was clearly different to the CoNC system (Figure S16). This result provided evidence for tuned oxidation pathways and catalytic mechanisms after integration of iron metal atoms into the CoNC configuration. Additionally, in the LC-MS spectra, a large proportion of TC was still preserved in the CoNC/PMS system, while the characteristic peak of TC almost disappeared after 20 min under the attack of FeCoNC catalyst, indicating efficiently promoted oxidation and mineralization ability. Furthermore, the anti-interference ability and applicability of FeCoNC catalyst were evaluated under high concentration of anions, tap water and actual wastewater, which was harvested from the effluent of Tokyo

Sewerage system in Tokyo, Japan. As depicted in Figure 6d, the presence of Cl^-, NO_3^-, PO_4^- and humic acid (HA) slightly suppressed the TC degradation by the FeCoNC/PMS system. The inhibitory effect was mainly attributed to free radical quenching by these anions to form less reactive species and the coverage of adsorption/activation sites for PMS[51, 52]. On the contrary, not only did the introduction of CO_3^{2-} not deactivate the catalytic efficiency, but it accelerated the degradation process, which was mainly derived from the modification of solution pH by the CO_3^{2-} ions. Moreover, after dissolving TC in tap water and actual wastewater, 76.7 % and 71.8% degradation of TC was still accomplished by FeCoNC catalyst within 30 min (Figure 6e). The TOC removal rate achieved 55.4% after the first cycle and FeCoNC-2 maintained approximately 93% of its original catalytic capacity after five cyclic tests, indicating the excellent reactivity and favorable application potential in future environmental purification. By contrast, the catalytic performance significantly declined in the CoNC/PMS system after five cycles and the leached Co ion was measured to be 0.73 mg L^{-1}, which was far higher than that of FeCoNC catalyst (0.031 mg L^{-1}, Figure S17). The introduction of iron atoms in the CoNC catalyst not only improved the catalytic ability but stabilized the intermetallic bonding interaction, which made it difficult for the metal ions to escape and deactivate from the structure[53]. These analyses reflected the superior stability and application feasibility of FeCoNC catalyst in PMS-AOPs based wastewater treatment.

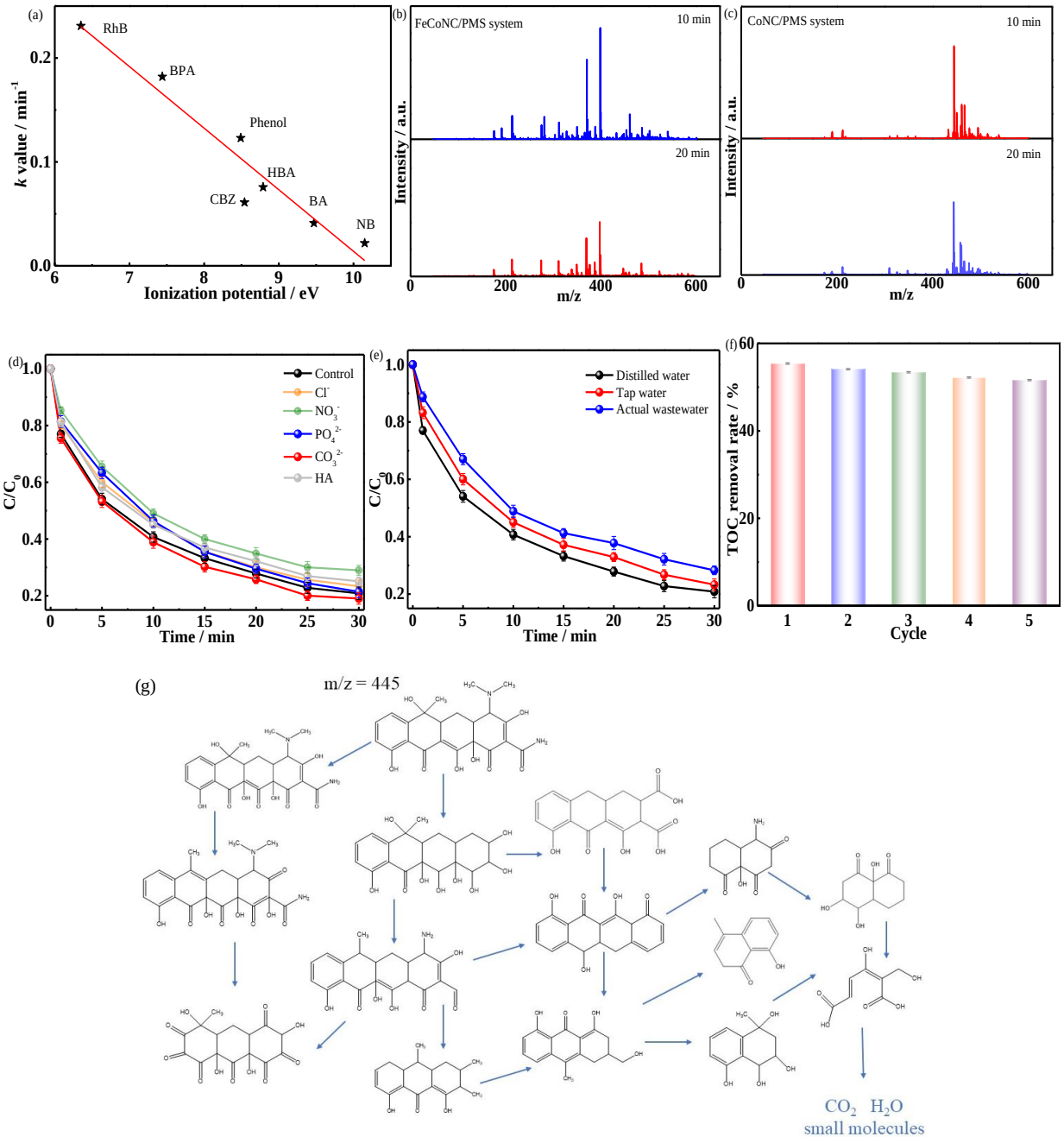

Figure 6. (a) The relationship between the catalytic activity and IP value; (b-c) MS spectra of TC decomposition in FeCoNC and CoNC systems; (d) Effect of common inorganic anions and humic acid on TC degradation in FeCoNC-2/PMS system; (e) TC oxidation in tap water and actual wastewater; (f) TOC removal rate in actual wastewater by FeCoNC-2 catalyst; (g) Possible degradation pathways of TC in FeCoNC/PMS system; Reaction conditions: catalyst dosage = 0.3 g/L, $[PMS]_0$ = 2.0 mM, $[TC]_0$ = 80 mg/L, $[Cl^-]_0 = [NO_3^-]_0 = [PO_4^{2-}]_0 = [CO_3^{2-}]_0$ = 10.0 mM, $[HA]_0$ = 10 mg/L;

Conclusion

This work illustrated heterogeneous catalysts featuring two bonded Fe-Co dual atoms, which can be well represented by an N_3-Fe-Co-N_3 structural ensemble with 100% metal dispersion in N-doped carbon support. Benefiting from its unique electron structure and synergistic effects of Fe-Co dual sites, the FeCoNC catalyst showed excellent catalytic activity and stability for PMS activation and TC oxidation, which was promoted about by 13.5 times compared with its CoNC catalyst counterpart. EPR measurements and scavenging experiments manifested nonradical singlet oxygen as the dominant reactive species in both systems, while the formation pathways of $^1O_2$ and catalysis processes were distinctly different. The combination of Mössbauer spectroscopy and theoretical calculation revealed the dynamic electronic structure and increased covalency in Co-N bonds, inducing improved positive charge density, promoted electron transfer and enabling N_3-Fe-Co-N_3 configuration as the major active sites to lower the PMS activation barriers. The optimized structure achieved by introducing Fe atoms into CoNC catalyst resulted in significant capacity and stability enhancement during PMS-AOPs reaction. This work provided meaningful insights into the generation and transformation mechanism of dual atomic metal sties and had profound implications for PMS-AOPs based green environmental remediation processes.

Acknowledgements

This work was supported by the Tokyo Human Resources Fund for City Diplomacy (H29-1).

References

[1] J. Lee, U. von Gunten, J.H. Kim, Persulfate-Based Advanced Oxidation: Critical Assessment of Opportunities and Roadblocks, Environ. Sci. Technol., 54 (2020) 3064-3081.

[2] N. Thomas, D.D. Dionysiou, S.C. Pillai, Heterogeneous Fenton catalysts: A review of recent advances, J Hazard Mater., 404 (2021) 124082.

[3] X. Zhou, Q. Zhao, J. Wang, Z. Chen, Z. Chen, Nonradical oxidation processes in PMS-based heterogeneous catalytic system: Generation, identification, oxidation characteristics, challenges response and application prospects, Chem. Eng. J., 410 (2021) 128312.

[4] W. Miao, Y. Liu, D. Wang, N. Du, Z. Ye, Y. Hou, S. Mao, K. Ostrikov, The role of Fe-N_x single-atom catalytic sites in peroxymonosulfate activation: Formation of surface-activated complex and non-radical pathways, Chem. Eng. J., 423 (2021) 130250.

[5] J. Miao, W. Geng, P.J.J. Alvarez, M. Long, 2D N-Doped Porous Carbon Derived from Polydopamine-Coated Graphitic Carbon Nitride for Efficient Nonradical Activation of Peroxymonosulfate, Environ. Sci. Technol., 54 (2020) 8473-8481.

[6] C. Song, Q. Zhan, F. Liu, C. Wang, H. Li, X. Wang, X. Guo, Y. Cheng, W. Sun, L. Wang, J. Qian, B. Pan, Overturned Loading of Inert CeO_2 to Active Co_3O_4 for Unusually Improved Catalytic Activity in Fenton-Like Reactions, Angew. Chem., Int. Ed. Engl., (2022) e202200406.

[7] N. Du, Y. Liu, Q. Li, W. Miao, D. Wang, S. Mao, Peroxydisulfate activation by atomically-dispersed Fe-N_x on N-doped carbon: Mechanism of singlet oxygen evolution for nonradical degradation of aqueous contaminants, Chem. Eng. J., 413 (2021) 127545.

[8] C. Jia, Q. Wang, J. Yang, K. Ye, X. Li, W. Zhong, H. Shen, E. Sharman, Y. Luo, J. Jiang, Toward Rational Design of Dual-Metal-Site Catalysts: Catalytic Descriptor Exploration, ACS Catal., 12 (2022) 3420-3429.

[9] S. Liu, D. Liu, Y. Sun, P. Xiao, H. Lin, J. Chen, X. L. Wu, X. Duan, S. Wang, Enzyme-mimicking single-atom FeN_4 sites for enhanced photo-Fenton-like reactions, Appl. Catal., B, 310 (2022) 121327.

[10] H. Huang, D. Yu, F. Hu, S. C. Huang, J. Song, H. Y. Chen, L.L. Li, S. Peng, Clusters Induced Electron Redistribution to Tune Oxygen Reduction Activity of Transition Metal Single-Atom for Metal–Air Batteries, Angew. Chem., Int. Ed. Engl., 61 (2022) e202116068.

[11] L. Deng, F. Hu, M. Ma, S. C. Huang, Y. Xiong, H. Y. Chen, L. Li, S. Peng, Electronic Modulation Caused by Interfacial Ni-O-M (M=Ru, Ir, Pd) Bonding for Accelerating Hydrogen Evolution Kinetics, Angew. Chem., Int. Ed. Engl., 60 (2021) 22276-22282.

[12] J. Wang, B. Li, Y. Li, X. Fan, F. Zhang, G. Zhang, W. Peng, Facile Synthesis of Atomic Fe-N-C Materials and Dual Roles Investigation of Fe-N_4 Sites in Fenton-Like Reactions, Adv. Sci., 8 (2021) e2101824.

[13] X. Zhang, B. Xu, S. Wang, X. Li, C. Wang, B. Liu, F. Han, Y. Xu, P. Yu, Y. Sun, Tetracycline degradation by peroxymonosulfate activated with CoN_x active sites: Performance and activation mechanism, Chem. Eng. J., 431 (2022) 133477.

[14] T. Cui, Y.P. Wang, T. Ye, J. Wu, Z. Chen, J. Li, Y. Lei, D. Wang, Y. Li, Engineering Dual Single-Atom Sites on 2D Ultrathin N-doped Carbon Nanosheets Attaining Ultra-Low-Temperature Zinc-Air Battery, Angew. Chem., Int. Ed. Engl., 61 (2022) e202115219.

[15] N.K. Wagh, D.H. Kim, S.H. Kim, S.S. Shinde, J.H. Lee, Heuristic Iron-Cobalt-Mediated Robust pH-Universal Oxygen Bifunctional Lusters for Reversible Aqueous and Flexible Solid-State Zn-Air Cells, ACS Nano, 15 (2021) 14683-14696.

[16] D. Yu, Y. Ma, F. Hu, C.-C. Lin, L. Li, H. Y. Chen, X. Han, S. Peng, Dual-Sites Coordination Engineering of Single Atom Catalysts for Flexible Metal–Air Batteries, Angew. Chem., Int. Ed. Engl., 11 (2021) 2101242.

[17] L. Li, D. Yu, P. Li, H. Huang, D. Xie, C. C. Lin, F. Hu, H. Y. Chen, S. Peng, Interfacial electronic coupling of ultrathin transition-metal hydroxide nanosheets with layered MXenes as a new prototype for platinum-like hydrogen evolution, Energy Environ. Sci., 14 (2021) 6419-6427.

[18] F. Hu, D. Yu, M. Ye, H. Wang, Y. Hao, L. Wang, L. Li, X. Han, S. Peng, Lattice-Matching Formed Mesoporous Transition Metal Oxide Heterostructures Advance Water Splitting by Active Fe–O–Cu Bridges, Adv. Energy Mater., 12 (2022) 2200067.

[19] Y. He, X. Yang, Y. Li, L. Liu, S. Guo, C. Shu, F. Liu, Y. Liu, Q. Tan, G. Wu, Atomically Dispersed Fe–Co Dual Metal Sites as Bifunctional Oxygen Electrocatalysts for Rechargeable and Flexible Zn–Air Batteries, ACS. Catal., (2022) 1216-1227.

[20] M. Jiang, F. Wang, F. Yang, H. He, J. Yang, W. Zhang, J. Luo, J. Zhang, C. Fu, Rationalization on high-loading iron and cobalt dual metal single atoms and mechanistic insight into the oxygen reduction reaction, Nano Energy, 93 (2022) 106793.

[21] C. Gao, J. Low, R. Long, T. Kong, J. Zhu, Y. Xiong, Heterogeneous Single-Atom Photocatalysts: Fundamentals and Applications, Chem. Rev., 120 (2020) 12175-12216.

[22] K. Qian, H. Chen, W. Li, Z. Ao, Y.N. Wu, X. Guan, Single-Atom Fe Catalyst Outperforms Its Homogeneous Counterpart for Activating Peroxymonosulfate to Achieve Effective Degradation of Organic Contaminants, Environ. Sci. Technol., 55 (2021) 7034-7043.

[23] W. Ren, G. Nie, P. Zhou, H. Zhang, X. Duan, S. Wang, The Intrinsic Nature of Persulfate Activation and N-Doping in Carbocatalysis, Environ. Sci. Technol., 54 (2020) 6438-6447.

[24] Y. Wu, C. Ye, L. Yu, Y. Liu, J. Huang, J. Bi, L. Xue, J. Sun, J. Yang, W. Zhang, X. Wang, P. Xiong, J. Zhu, Soft template-directed interlayer confinement synthesis of a Fe-Co dual single-atom catalyst for Zn-air batteries, Energy Storage Mater., 45 (2022) 805-813.

[25] J. Yang, D. Zeng, J. Li, L. Dong, W. J. Ong, Y. He, A highly efficient Fenton-like catalyst based on isolated diatomic Fe-Co anchored on N-doped porous carbon, Chem. Eng. J., 404 (2021) 126376.

[26] U.I. Kramm, L. Ni, S. Wagner, ^{57}Fe Mossbauer Spectroscopy Characterization of Electrocatalysts, Adv. Mater., 31 (2019) e1805623.

[27] W. Liu, L. Zhang, X. Liu, X. Liu, X. Yang, S. Miao, W. Wang, A. Wang, T. Zhang, Discriminating Catalytically Active FeNx Species of Atomically Dispersed Fe-N-C Catalyst for Selective Oxidation of the C-H Bond, J. Am. Chem. Soc., 139 (2017) 10790-10798.

[28] U.I. Kramm, J. Herranz, N. Larouche, T.M. Arruda, M. Lefevre, F. Jaouen, P. Bogdanoff, S. Fiechter, I. Abs-Wurmbach, S. Mukerjee, J.P. Dodelet, Structure of the catalytic sites in Fe/N/C-catalysts for O_2-reduction in PEM fuel cells, Phys. Chem. Chem. Phys., 14 (2012) 11673-11688.

[29] E. Kuzmann, Z. Homonnay, Z. Klencsar, R. Szalay, ^{57}Fe Mossbauer Spectroscopy as a Tool for Study of Spin States and Magnetic Interactions in Inorganic Chemistry, Molecules, 26 (2021) 1062.

[30] B. Zhang, X. Li, K. Akiyama, P.A. Bingham, S. Kubuki, Elucidating the Mechanistic Origin of a Spin State-Dependent FeN_x-C Catalyst toward Organic Contaminant Oxidation via Peroxymonosulfate Activation, Environ. Sci. Technol., 56 (2022) 1321-1330.

[31] I. Yamada, A. Takamatsu, N. Hayashi, H. Ikeno, Covalency Competition in the Quadruple Perovskite $CdCu_3Fe_4O_{12}$, Inorg. Chem., 56 (2017) 9303-9310.

[32] J. Hu, Y. Li, Y. Zou, L. Lin, B. Li, X. y. Li, Transition metal single-atom embedded on N-doped carbon as a catalyst for peroxymonosulfate activation: A DFT study, Chem. Eng. J., 437 (2022) 135428.

[33] Z. Wang, C. Lai, L. Qin, Y. Fu, J. He, D. Huang, B. Li, M. Zhang, S. Liu, L. Li, W. Zhang, H. Yi, X. Liu, X. Zhou, ZIF-8-modified $MnFe_2O_4$ with high crystallinity and superior photo-Fenton catalytic activity by Zn-O-Fe structure for TC degradation, Chem. Eng. J., 392 (2020) 124851.

[34] R. Tang, D. Gong, Y. Deng, S. Xiong, J. Zheng, L. Li, Z. Zhou, L. Su, J. Zhao, π-π stacking derived from graphene-like biochar/g-C_3N_4 with tunable band structure for photocatalytic antibiotics degradation via peroxymonosulfate activation, J. Hazard. Mater., 423 (2022) 126944.

[35] L. Yang, H. Yang, S. Yin, X. Wang, M. Xu, G. Lu, Z. Liu, H. Sun, Fe Single-Atom Catalyst for Efficient and Rapid Fenton-Like Degradation of Organics and Disinfection against Bacteria, Small, 18 (2022) e2104941.

[36] S. Liu, Z. Zhang, F. Huang, Y. Liu, L. Feng, J. Jiang, L. Zhang, F. Qi, C. Liu, Carbonized polyaniline activated peroxymonosulfate (PMS) for phenol degradation: Role of PMS adsorption and singlet oxygen generation, Appl. Catal., B, 286 (2021) 119921.

[37] P. Duan, J. Pan, W. Du, Q. Yue, B. Gao, X. Xu, Activation of peroxymonosulfate via mediated electron transfer mechanism on single-atom Fe catalyst for effective organic pollutants removal, Appl. Catal., B, 299 (2021) 120714.

[38] C. Dong, Y. Bao, T. Sheng, Q. Yi, Q. Zhu, B. Shen, M. Xing, I.M.C. Lo, J. Zhang, Singlet oxygen triggered by robust bimetallic MoFe/TiO_2 nanospheres of highly efficacy in solar-light-driven peroxymonosulfate activation for organic pollutants removal, Appl. Catal., B, 286 (2021) 119930.

[39] H. Wang, W. Guo, B. Liu, Q. Wu, H. Luo, Q. Zhao, Q. Si, F. Sseguya, N. Ren, Edge-nitrogenated biochar for efficient peroxydisulfate activation: An electron transfer mechanism, Water Res., 160 (2019) 405-414.

[40] X. Liang, D. Wang, Z. Zhao, T. Li, Z. Chen, Y. Gao, C. Hu, Engineering the low-coordinated single cobalt atom to boost persulfate activation for enhanced organic pollutant oxidation, Appl. Catal., B, 303 (2022) 120877.

[41] P. Zhang, Y. Yang, X. Duan, Y. Liu, S. Wang, Density Functional Theory Calculations for Insight into the Heterocatalyst Reactivity and Mechanism in Persulfate-Based Advanced Oxidation Reactions, ACS Catal., 11 (2021) 11129-11159.

[42] Y. Yang, P. Zhang, K. Hu, X. Duan, Y. Ren, H. Sun, S. Wang, Sustainable redox processes induced by peroxymonosulfate and metal doping on amorphous manganese dioxide for nonradical degradation of water contaminants, Appl. Catal., B, 286 (2021) 119903.

[43] G. Kresse, J. Furthmüller, Efficient iterative schemes for ab initio total-energy calculations using a plane-wave basis set, Phys. Rev. B, 54 (1996) 11169-11186.

[44] C. Liu, T. Li, X. Dai, J. Zhao, D. He, G. Li, B. Wang, X. Cui, Catalytic Activity Enhancement on Alcohol Dehydrogenation via Directing Reaction Pathways from Single- to Double-Atom Catalysis, J. Am. Chem. Soc., 144 (2022) 4913-4924.

[45] W. Ren, C. Cheng, P. Shao, X. Luo, H. Zhang, S. Wang, X. Duan, Origins of Electron-Transfer Regime in Persulfate-Based Nonradical Oxidation Processes, Environ. Sci. Technol., 56 (2022) 78-97.

[46] S. Zhu, X. Li, J. Kang, X. Duan, S. Wang, Persulfate Activation on Crystallographic Manganese Oxides: Mechanism of Singlet Oxygen Evolution for Nonradical Selective Degradation of Aqueous Contaminants, Environ. Sci. Technol., 53 (2019) 307-315.

[47] P. Hu, H. Su, Z. Chen, C. Yu, Q. Li, B. Zhou, P.J.J. Alvarez, M. Long, Selective Degradation of Organic Pollutants Using an Efficient Metal-Free Catalyst Derived from Carbonized Polypyrrole via Peroxymonosulfate Activation, Environ. Sci. Technol., 51 (2017) 11288-11296.

[48] X. Zhang, B. Xu, S. Wang, X. Li, C. Wang, B. Liu, F. Han, Y. Xu, P. Yu, Y. Sun, Tetracycline degradation by peroxymonosulfate activated with CoN_x active sites: Performance and activation mechanism, Chem. Eng. J., 431 (2022) 133477.

[49] Z. J. Xiao, X. C. Feng, H.T. Shi, B. Q. Zhou, W. Q. Wang, N. Q. Ren, Why the cooperation of radical and non-radical pathways in PMS system leads to a higher efficiency than a single pathway in tetracycline degradation, J. Hazard. Mater., 424 (2022) 127247.

[50] S. Liu, Y. Liu, M. Chen, L. Li, W. Tu, Z. Huang, $CuFe_2O_4$ modified expanded graphite synthesized by urea-assisted hydrothermal method for tetracycline treatment through persulfate activation: Characterization, mechanism and degradation intermediates, Chem. Eng. J., 433 (2022) 133516.

[51] V.K. Sharma, M. Feng, D.D. Dionysiou, H.C. Zhou, C. Jinadatha, K. Manoli, M.F. Smith, R. Luque, X. Ma, C.H. Huang, Reactive High-Valent Iron Intermediates in Enhancing Treatment of Water by Ferrate, Environ. Sci. Technol., 56 (2022) 30-47.

[52] R. Luo, M. Li, C. Wang, M. Zhang, M.A. Nasir Khan, X. Sun, J. Shen, W. Han, L. Wang, J. Li, Singlet oxygen-dominated non-radical oxidation process for efficient degradation of bisphenol A under high salinity condition, Water Res., 148 (2019) 416-424.

[53] J. Wang, W. Liu, G. Luo, Z. Li, C. Zhao, H. Zhang, M. Zhu, Q. Xu, X. Wang, C. Zhao, Y. Qu, Z. Yang, T. Yao, Y. Li, Y. Lin, Y. Wu, Y. Li, Synergistic effect of well-defined dual sites boosting the oxygen reduction reaction, Energy Environ. Sci., 11 (2018) 3375-3379.